Journal of Energy Storage 124 (2025) 116812

Contents lists available at ScienceDirect

Journal of Energy Storage

journal homepage: www.elsevier.com/locate/est

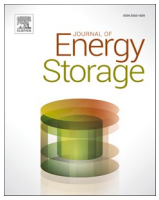

Research papers

Transfer from experimental test cell to automotive pouch cell level: A combined experimental and modeling approach

Anne Heß *, Thomas Wetzel, Philipp Seegert

Karlsruhe Institute of Technology (KIT), Institute of Thermal Process Engineering (TVT), Heat and Mass Transfer, 76131 Karlsruhe, Germany

ARTICLE INFO

Keywords:
Lithium-ion battery
Experimental cells
Parameterization
Pouch cells
Impedance-based equivalent circuit modeling
Voltage prediction
Fast charging strategies

ABSTRACT

Knowledge of the local electrode potentials within the battery cell is essential for a safe and optimal operating window, as well as innovative fast charging strategies of lithium-ion batteries. Three-electrode test cells facilitate measuring the individual electrode's behavior during operation. However, transferring test cell results to large-scale commercial (pouch) cells is not straightforward. In this paper, we investigate the comparison of an automotive 60 Ah pouch cell with three-electrode cells built out of extracted electrodes from the pouch cell and standard components for the separator and electrolyte, using a commercial test cell housing. We found that the measured voltage behavior of both cell types differs significantly for C-rates higher than C/4 and fast changing current loads, such as pulse profiles or Worldwide Harmonized Light Vehicles Test Procedure cycles. This discrepancy hinders the direct transfer of test cell results to large pouch cells. To address this issue, we introduced an equivalent circuit model that incorporates an ohmic correction factor to bridge the experimental data and pouch cell behavior. The model's parameters are derived from the half-cell impedance data measured, enabling the investigation of local potentials at the anode and cathode within the simulation framework. We achieved a good correlation and reproducibility for rapidly changing current loads. The methodology presented demonstrates a good potential for fast and significant parametrization of simulation models by utilizing the extracted electrode material of the pouch cell and easily obtainable standard separators and electrolytes with a very high reproducibility.

1. Introduction

A profound knowledge of the behavior of both electrodes within a lithium-ion battery is necessary for a fundamental understanding of the battery cell's performance. The anode is a limiting factor especially for certain operations, such as fast charging, due to lithium plating when the potential at the anode drops below 0 V *vs.* Li/Li^+ [1–3]. The knowledge of local processes is crucial for the determination of safe and optimal operating windows on a cell level. The use of simulation models based on the individual half-cell behavior of the anode and cathode enables an efficient and targeted optimization process of the battery performance. Optimized fast charging conditions and loading profiles, for example, could be derived with a deeper understanding of the local anode behavior.

There is no simple way to measure the individual electrode behavior within commercial cells, such as automotive pouch cells, during operation. Therefore, lab scale cell formats, such as experimental cells (three-electrode test cells), are useful and widespread tools for investigations of the electrodes in the context of the full cell behavior. Different formats in lab scale, such as coin cells [4–14], to which the experimental cells belong, or single layer [11–13] and multilayer pouch cells [5,9–11,13,14], are used for systematic investigations on the electrode level. The individual components, such as the electrolyte, active materials or separator, can be varied easily and, thus, different setups can be investigated.

The same electrode, electrolyte and separator materials are used for the assembly of different cell formats, and the performances, considering the different formats, are compared in many studies [5,10–12,14]. Mostly pristine materials are used for the experimental setup, but in the case of the electrodes, they can also be extracted from commercial cells through careful cell opening and preparation. However, regarding commercial automotive cells, the exact configuration of the electrolyte and separator are, in most cases, unknown and the replication of these in experimental setups is not easily achieved. Companies, such as EL-Cell GmbH, offer cell housings and standardized components, including separators and reference electrodes, for the reliable and significant

* Corresponding author.
E-mail address: anne.hess@kit.edu (A. Heß).

https://doi.org/10.1016/j.est.2025.116812
Received 26 November 2024; Received in revised form 7 March 2025; Accepted 26 April 2025
Available online 2 May 2025

performance of experimental cells. Three-electrode setups can be built with these components, the electrodes extracted from the commercial cell and the behavior of the individual electrodes measured.

Nonetheless, quite high differences regarding the cell area and, therefore, the capacity as well as the resistance of the experimental and the pouch cell exist, and the question arises to what extent conclusions from the experimental cell with a standard separator and electrolyte can be drawn to the commercial pouch cell.

To the best of the authors' knowledge, a profound comparison of the behavior of experimental cells to commercial cells and a transfer of the insights gained for the modeling of the commercial cell behavior on the basis of experimental cell parameterization can only be found to a quite small extent in literature. In cases where experimental cells are used for the parametrization of models of commercial cells, the impedance data of the experimental cells is simply multiplied by an area scaling factor [15]. The experimental data is more often used for a direct modeling of only the experimental cells and not the commercial cell or to gain parameters of the electrode materials [16,17]. A general experimental analysis of differences between pouch and coin cells is shown by Son et al. [14] and, as a result, the difference in the scale of the impedance is named as the main cause for differences in the rate performance. However, there is no mention of what consequences this could have for modeling the pouch cell using the coin cell data. In more cases, a broader comparison of different cell formats is shown [5,9,11,12], again comparing only experimental data. Hereby, the coin cells are often used as a reference and for pretesting the electrodes, and the best variants are then assembled in pouch cells. The degradation behavior of commercial cells and coin cells are experimentally compared in some aging studies [18] but with the result that coin cells are not suitable for the aging prediction of commercial cells.

Considering either an experimental or a modeling level, but not both at the same time, is common in all works found. Furthermore, a setup with standardized components for the experimental cells is rarely used when considering different formats. Additionally, possible causes and resulting effects of the differences in the setup of the cells and their performance are only mentioned to a very limited extent.

In this work, we show a systematic experimental comparison of the pouch cell and experimental cell behavior. We discuss under which operation conditions, such as C-rate and temperature, conclusions can be drawn from the experimental compared to the pouch cell. The measurement of significant half-cell impedance spectra for the individual electrodes is presented and it is shown that the combination of the half-cell impedances resembles the full cell behavior correctly. Thereby, the inductive loop in the impedance of the individual electrodes of experimental cell setups, as observed in the literature [19–25], and its causes are investigated.

Furthermore, we introduce a correction factor to align the behavior of the experimental coin cell to the automotive pouch cell, which is a useful tool for the simulation of a pouch cell with half-cell-based data of the experimental cells. The simulation model developed is described and the pivotal results are shown and discussed.

The study presented shows the possibility of the simulation of a pouch cell parameterized with upscaled experimental cell data, which offers the opportunity to draw conclusions about the individual electrodes in operation and, thus, reveal the respective limitations in different operating scenarios.

2. Experimental investigations

2.1. Experimental setup – pouch cell

We investigated a commercial automotive pouch cell with 60 Ah capacity, a graphite anode and NMC cathode (Table 1). The pouch cell was placed between two individually designed, flowed through, temperature control plates, which are connected to a cryostat (RE1050, LAUDA Dr. R. WOBSER GMBH & CO. KG) to be able to set the temperature precisely directly on the cell surface. The experiments were carried out in a VT^3 4018 (Vötsch Industrietechnik GmbH) climate chamber to provide a stable temperature environment and safety throughout the experiments.

Table 1
Specifications of the pouch and experimental cells.

	Pouch cell	Experimental cell
Capacity	60 Ah	7.49 mAh
Cell Area	20,363.20 cm^2	2.544 cm^2
Voltage range U_{min} - U_{max}	2.5–4.2 V	2.5–4.2 V

The cell was cycled using a CTS and XCTS (BaSyTec GmbH, Asselfingen, Germany) battery cell cycler. Electrochemical impedance spectroscopy (EIS) measurements were carried out with a Zahner Zennium (ZAHNER-elektrik GmbH & Co. KG, Kronach, Germany) extended with a power potentiostat PP241 in galvanostatic mode.

The pouch cell was exposed to 20 CCCV cycles with C/5 at the beginning of the testing procedure. Afterwards, EIS measurements at four different temperatures (0, 10, 25 and 45 °C) and various states of charge (SoCs) (0, 5, 10, 20, … 90, 95, 100 %) were carried out.

Different temperatures were chosen, because the underlying electrochemical processes like polarization and diffusion are strongly temperature-dependent and follow mainly Arrhenius law [26].

Additionally, measurements, such as dynamic profiles (Worldwide Harmonized Light-duty Vehicles Test Procedure: WLTP) and pulses, as well as constant current charge and discharge cycles were performed.

At the end of the whole measurement procedure, the pouch cell was discharged with C/10 to the minimum voltage of 2.5 V for preparation of the cell opening procedure to build the experimental cells.

2.2. Experimental setup – experimental cells

The discharged pouch cell was opened in an argon-filled glovebox and several anode and cathode sheets were carefully separated and immediately cleaned with dimethyl carbonate. In a next step, the active material on one side of each dried electrode sheet was removed using N-Methyl-2-pyrrolidone. Then, coins with a diameter of 18 mm were punched out.

The PAT-Cell housing from EL-Cell GmbH [27] is used for all experimental cells (Table 1) investigated. The commercial set-up from EL-Cell was chosen because of the minimization of the misalignment of the electrode with the PAT-Core system and a defined stacking pressure. The insulation sleeve used has a built-in 220 µm PP fiber/PE membrane separator and lithium reference ring. An 80 µl standard 1 M lithium hexafluorophosphate (LiPF6) dissolved in dimethyl carbonate (LP30, Sigma-Aldrich) was used as the electrolyte.

Regarding the full cells, the cathode was used as the lower electrode in the setup and the anode as the upper electrode. Accordingly, two anodes or two cathodes with the same SoC were used for the symmetrical cells.

The experimental cells were cycled with a BaSyTec CTS XL Lab and the impedance spectra were recorded using a Zahner® Zennium PRO electrochemical workstation extended by a PMUX-S cell multiplexer.

Coin cells in full cell configuration often do not exhibit reliable and reproducible behavior in the literature [6,8]. To avoid these problems and achieve significant measurement results, in addition to the careful assembly, a unified standard cycling protocol was performed with each cell, so that reproducible capacitances and impedances were achieved.

Afterwards, EIS measurements at four different temperatures (0, 10, 25 and 45 °C) and various SoCs were carried out. Additionally, the same measurement procedures of the pouch cell (WLTP, pulses, constant current charge and discharge cycles) were performed with the experimental cells.

2.3. Measurement techniques

In order to obtain the open-circuit voltage (OCV), C/40 measurements were performed, and the quasi-OCV (q-OCV) gained was used instead of time-consuming potentiometric measurements.

The cells were stabilized before each EIS measurement until the voltage gradient was less than 5 mV/h to avoid unsteady conditions. The time required for this was at least 60 min or, in the longest case, 180 min. The measurements were performed in galvanostatic mode, whereby linearity was assured by choosing a perturbation amplitude, so that the resulting voltage amplitude was lower than 10 mV. The frequency range was 100 kHz down to 5 mHz. Eleven steps per decade and 40 measuring periods for frequencies above 66 Hz and five steps per decade and 4 measuring periods for frequencies below 66 Hz were chosen for all impedance measurements. These settings led to a measurement duration of 80 min for each impedance spectrum. The chronological order of the EIS measurements of the experimental cells for each measurement point was: full cell, cathode and anode. Hereby, the half-cell spectra were measured directly after the previous measurement.

3. Modeling approach

The pouch cell behavior is simulated with an impedance-based approach. Therefore, the OCVs and impedances of the anode and cathode of the experimental cells at different SoCs and temperatures are needed from experimental characterization. Accordingly, a state-of-the-art modeling approach, consisting of a combination of ohmic resistances and RC elements, is used, similar to other approaches from literature [28–30].

Regarding the fitting of the measured impedances, an approach with ohmic resistance, an RQ element and a transition line model (TLM) is used for the anode and cathode, similar to established models from literature [17,31]. The chosen impedance fit accordingly takes into account the ohmic, polarization and diffusion processes, whereby the knowledge of the diffusion depends on the selected minimum frequency of the experimental data. The calculation of the TLM-impedance is determined with the formula according to Illig et al. [16]:

$$Z_{\mathrm{TLM}} = \frac{\chi_1\chi_2}{\chi_1+\chi_2}\left(L + \frac{2\kappa}{\sinh\left(\frac{L}{\kappa}\right)}\right) + \kappa\frac{\chi_1^2+\chi_2^2}{\chi_1+\chi_2}\coth\left(\frac{L}{\kappa}\right) \tag{1}$$

$$\kappa = \sqrt{\frac{\zeta}{\chi_1+\chi_2}} \tag{2}$$

The TLM offers the opportunity to include microstructure properties, such as porosity, and the electric and ionic conductivity, and is used for porous electrode structures [16,17,32–34]. These variables are used to calculate the distributed resistance elements χ_1 and χ_2, which represent the electronic and ionic path. The formula used for χ_1 and χ_2 as well as the parameters utilized are shown in Table 2.

The electrode thickness was measured with a mechanical gauge (Mahr Micromar 40 EWR with 0.001 mm resolution), and the porosity was determined from the weight measured, coin area, and electrode thickness and density. The other values were taken from literature, whereby the anode tortuosity used was particularly set on a chosen value, which lies within the range of the very scattered literature values.

Regarding the modeling of the anode and cathode, the only difference lies in the interface resistance ζ. The anode has an extra RQ element, which is due to the SEI [41,42]. This impedance model is based on RQ elements and the TLM cannot be used straight forwardly for a calculation of the losses in the time area. Therefore, an RC approximation is needed for these impedances. A least-square fit is performed for this conversion, where the difference between the impedance measured and the impedance calculated with 15 RC elements is minimized. As closing conditions, the overall resistance as well as the time constants of the fastest (RQ1) and slowest process (FLW) are used to ensure that the frequency behavior is equal.

Table 2
Formulas and parameters for the electronic and ionic path for the TLM model used. Parameters taken from literature are labeled accordingly. The remaining values were measured or calculated.

	Anode	Cathode
Electrode thickness L	70 µm	50 µm
Ion conductivity σ_{ion}	0.76 Sm^{-1} [16,35]	
Electronic conductivity $\sigma_{\mathrm{el,eff}}$	1000 Sm^{-1} [16,36,37]	29.7 Sm^{-1} [17,35]
Cell area A	2.54 cm^2	
Porosity ε	0.336	0.43
Tortuosity τ	3 [16,38–40]	1.5 [17,35,37]
$\chi_1 \cdot L = R_{\mathrm{el}} = \frac{1}{\sigma_{\mathrm{el,eff}}}\cdot\frac{L}{A}$	0.276 mΩ	6.63 mΩ
$\chi_2 \cdot L = R_{\mathrm{ion}} = \frac{1}{\sigma_{\mathrm{ion}}}\cdot\frac{L}{A}\cdot\frac{\tau}{\varepsilon}$	3.28 Ω	0.9 Ω

An overview of the equivalent circuit models (ECM) used and the resulting ECM containing only the ohmic resistance and RC elements is given in Fig. 1.

The resulting impedances, with Ω as the unit, have to be converted by an area-factor to be able to simulate the voltage behavior of the pouch cell. Therefore, the cell areas of both cell types as well as the R and C values are used according to the following equation:

$$R_{\mathrm{new}} = R\cdot\frac{A_{\mathrm{Coin}}}{A_{\mathrm{Pouch}}},\quad C_{\mathrm{new}} = C\cdot\frac{A_{\mathrm{Pouch}}}{A_{\mathrm{Coin}}} \tag{3}$$

Due to this conversion, the resulting time constant, which is defined by the multiplication of R and C, stays equal for each RC element. The values fitted for each element, depending on the SoC and temperature, are saved in look-up tables.

For the pouch cell simulation, the time-depending current, fix temperature and starting SoC are needed as input parameter. The model calculates in fixed time steps the development of the SoC and the voltage, whereby the according values of the RC elements for each SoC are calculated during the simulation with an interpolation of the values in the table. The output of the model is the resulting voltage.

The model described for the simulation of the voltage behavior of the pouch cell is capable in real-time and was implemented in MATLAB.

4. Results and discussion

4.1. Impedances of experimental cells

4.1.1. Addition of anode and cathode impedance

We compared the sum of both electrodes with the impedance of the experimental full cell for the verification of the impedances of the individual electrodes. Therefore, the impedance of the anode and cathode is added for every frequency point. The comparison of the different impedances measured at 25 °C for a 10 % SoC can be seen in Fig. 2.

A very good agreement between the combination by addition of both individual electrode measurements (combined full cell) and the full cell measurement can be seen. Merely a slight ohmic shift can be observed, which is consistent over the whole frequency range. This can be seen directly in the parallel shift of the red curve (full cell measurement) and the black curve (combined full cell based of the combination of the anode and cathode) in the Bode plot of the real part in Fig. 2 (c). This observation is consistent for all measurements under the conditions mentioned (Section 2.1), thus, only one example is shown here. This shift is probably due to the measurement of the reference electrode at the side of the separator and, therefore, not the real geometrical center of the separator. Nevertheless, this shift is only marginal and does not dominate the impedance.

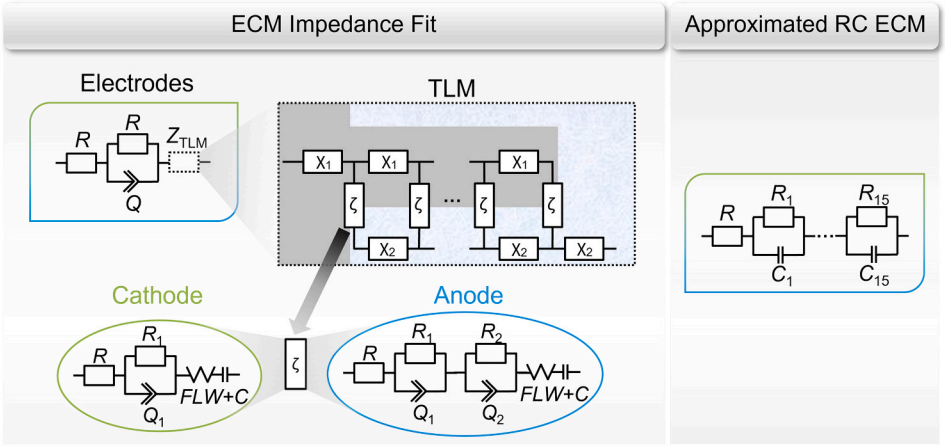

Fig. 1. Overview of the ECM used for the impedance fit and the resulting ECM after the ECM conversion for anode and cathode.

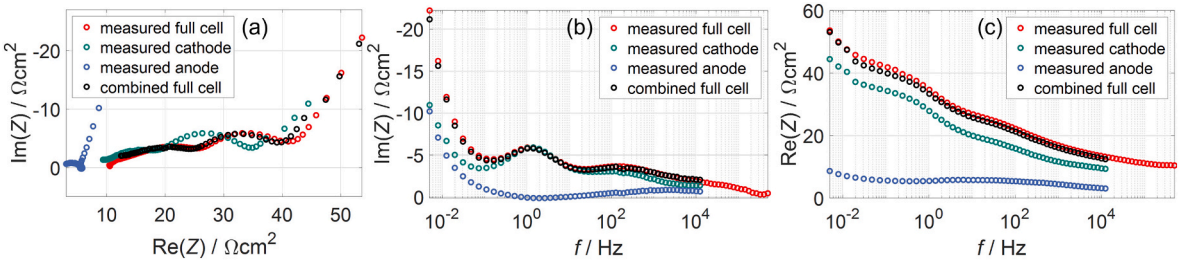

Fig. 2. Comparison of the full cell impedance measured and the sum of the anode and cathode impedance measured for 25 °C and 10 % SoC (a) in the form of a Nyquist plot, (b) as a Bode plot of the imaginary part and (c) as a Bode plot of the real part.

Due to the individual measurements of the single electrodes, the contribution of these to the overall full cell performance can be seen and conclusions can be drawn regarding at which operation point which electrode is the limiting factor. It is very clear in the results shown that the cathode impedance is the cause of the main loss process of the full cell, and, therefore, dominates the impedance for low SoCs.

In summary, these results show that it is legitimate to calculate the full cell impedance based on the combination of the anode and cathode impedances, which are measured with the assembly presented. However, it should be noted that it is not possible to measure quite as high frequencies in the half-cells as in the full cell configuration without obtaining artifacts, which is probably due to the Li reference electrode ring.

This finding leads, as a logical consequence, to the second result, that it is also legitimate to measure the full cell impedance and only one of both half-cell impedances and calculate the second half-cell out of both these measurements. Therefore, only two impedance measurements for each operating point are sufficient.

4.1.2. *Low-frequency inductive loop*

A low-frequency loop can be observed especially at anode spectra. Since this loop causes the imaginary part to become positive in a certain range, this loop is often called an inductive loop [19–25]. An example of impedances at 25 °C (a) and 10 °C (b) and different SoCs is given in Fig. 3.

This loop is pronounced to varying degrees depending on the SoC and temperature. The proportion of the loop in the total impedance increases significantly for lower temperatures. The magnitude of the loop decreases slightly with decreasing SoC and, therefore, a marginal influence of the SoC can be seen.

This low-frequency loop is observed by many groups and a high variety of different explanations for it are given. Possible origins, such as measurement errors due to imperfectly homogeneous electric fields to the reference electrode [43,44], multistage mechanisms of lithium

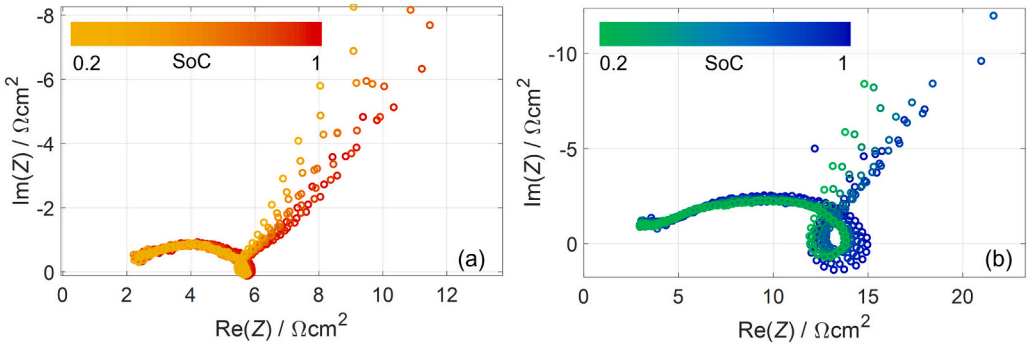

Fig. 3. Anode impedances for various SoCs between 20 and 100 % for (a) 25 °C and (b) 10 °C in the Nyquist plot.

intercalation [45], electrolyte impedance [46] and negative capacitance effects [47], are given.

As these inductive loops cannot be fitted by typical electrical equivalent circuit models, the question arises whether physical reactions are the cause, or only measurement influences are the origin.

At a first glance, the loop is only present in the anode spectra and is not visible in either the full cell or the cathode spectra. The first approach in this work was, therefore, to use the measurement of the cathode and full cell impedance for the calculation of the anode impedance.

The impedances measured and the anode and cathode calculated can be seen in Fig. 4.

In Fig. 4 (a) the overview of all impedance can be seen, whereas in Fig. 4 (b) only the cathodes and in Fig. 4 (c) only the anodes are shown. It is obvious that the calculated anode impedance also includes the inductive loop. This leads to the insight that an inductive loop also has to be present in the cathode impedance. When one zooms in on the area, a slight loop can also be seen in the cathode impedance, which is usually not visible due to the higher magnitude of the impedance in contrast to the anode.

The existence of this loop in the anode as well as the cathode spectra is a clear indication that it is not an actual physical process of the battery, but rather a metrological phenomenon of the experimental cell setup that only shows up when measurements of the lithium reference ring are performed. The loop is mathematically eliminated by adding the two spectra and the virtual full cell thus calculated shows, identical to the full cell directly measured, no low-frequency inductive loop.

Measurements with symmetrical cells were performed for verification to check whether the different magnitudes of the anode and cathode impedances could be the origin of the loop. Therefore, full cells were built and cycled with the standard protocol mentioned previously. At 50 % SoC, these cells were opened inside the glovebox and the anode and cathode extracted. These extracted electrodes were then used for the symmetrical cells.

Only a very slight form of a loop can be seen in the symmetrical cells with 50 % SoC on either electrode. The charge can be transferred between both electrodes in symmetrical cells, whereby two different SoCs of the electrodes can be achieved. With an exemplary shift of 25 % charge between two electrodes with originally 50 % SoC, one electrode reaches the 25 % SoC and the other 75 % SoC. Impedances at 0, 25, 50, 75 and 100 % SoC were measured with this method.

The impedances for each SoC of anodes (a) and cathodes (b) are shown in Fig. 5. The 0, 25 and 50 % SoCs are shown from the lower electrode in the setup of the symmetrical cell and the 75 and 100 % SoC from the upper electrode. The scale of the impedance for anodes with 0 % SoC is about five times the impedance at 100 % SoC. The same trend for the reversed SoC can be observed for the cathodes. A zoom into the area of the other impedances is shown for the better recognition of the loop.

The most pronounced loops can be observed in the electrodes with 100 % SoC for the anode and 0 % SoC for the cathode. The opposite electrodes had the 0 % SoC for the anode and 100 % SoC for the cathode. For these cases, the magnitudes of the impedances of the opposing electrodes differ the most.

The inductive loop can also be observed in symmetrical cells of the anode and cathode electrodes, whereby the size of the loop increases with the higher difference of the impedances between the opposing electrodes. This is an indication that the different magnitudes of the impedance between the upper and lower electrode is presumably one cause of the inductive loop, but not the only one.

To sum up these findings, the low-frequency loop is very likely not an electrode process. We assume that the different magnitudes of the impedances and the geometric position of the lithium reference ring in the experimental cell setup could be probable origins of this loop. Regarding the cell investigated, it can be concluded that the cathode dominates the losses and the visually relatively big inductive loop in the anode impedance spectra is not significant for the overall impedance behavior of the full cell.

4.2. Comparison of the impedance and performance of experimental and pouch cells

4.2.1. Impedance behavior

The measured impedances of experimental coin cells and automotive pouch cells were systematically compared for different temperatures and SoCs. As the pouch cell's impedance is strongly influenced at higher frequencies by the induction of the measurement setup (from the wiring *inter alia*), the visual comparison in the Nyquist plot initially leads to the impression that the impedances differ drastically from one another. The Bode plots of the real and imaginary part are additionally observed in order to resolve this.

The Nyquist plot and both Bode plots are shown, and the calculated differences in the real and imaginary part for every frequency point for two different SoCs at 25 °C are depicted in Fig. 6.

As mentioned above, the impedance looks very different in the Nyquist plot for both cell types and SoCs (50 % SoC in Fig. 6 (a) and 10 % SOC in Fig. 6 (f)). It becomes obvious in the Bode plot of the real part for a 50 % SoC (Fig. 6 b and d) that the real part has a nearly constant offset for a wide frequency area. The only exception are the high frequencies, where the impedance of the pouch cell is dominated by the measurement setup. The imaginary part of both cell types differs only for low and high frequencies and is identical for frequencies in a range of 0.05–50 Hz (Fig. 6 c and e). The same trend as described for the impedance data at SoC 50 % was also observed for SoCs between 30 and 95 % and 25 °C.

The results for decreasing SoC are shown exemplarily for 10 % SoC and 25 °C in Fig. 6 (f-j). As the SoC decreases, the difference in the imaginary part increases and is no longer nearly equal to zero (Fig. 6 j). Additionally, the real-part difference is no longer constant (Fig. 6 i). The deviation also increases for higher SoCs and temperatures, although to a much lower extent than for lower SoCs and temperatures. For high SoCs and temperatures, the contribution of lithium-ion transport in the electrolyte predominates the losses [16] and is, therefore, leading to the increasing difference between both cell formats with different electrolytes.

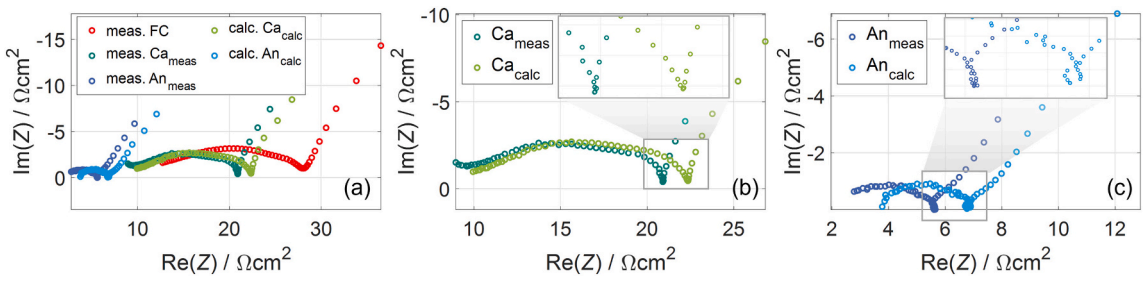

Fig. 4. Comparison of measured (meas.) and calculated (calc.) half-cell impedances in full cell (FC) configuration for 25 °C and 50 % SoC: overview of all spectra (a), cathode (Ca) spectra (b) and anode (An) spectra (c) in the Nyquist plot.

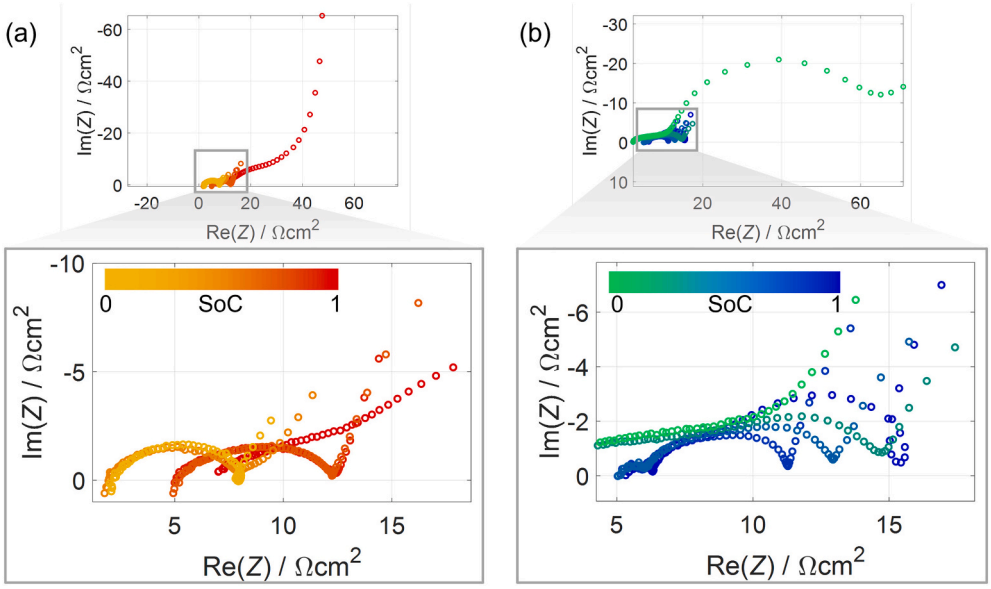

Fig. 5. Impedances of anodes (a) and cathodes (b) in symmetrical cells at 25 °C and 0, 25, 50, 75 and 100 % SoC in the Nyquist plot.

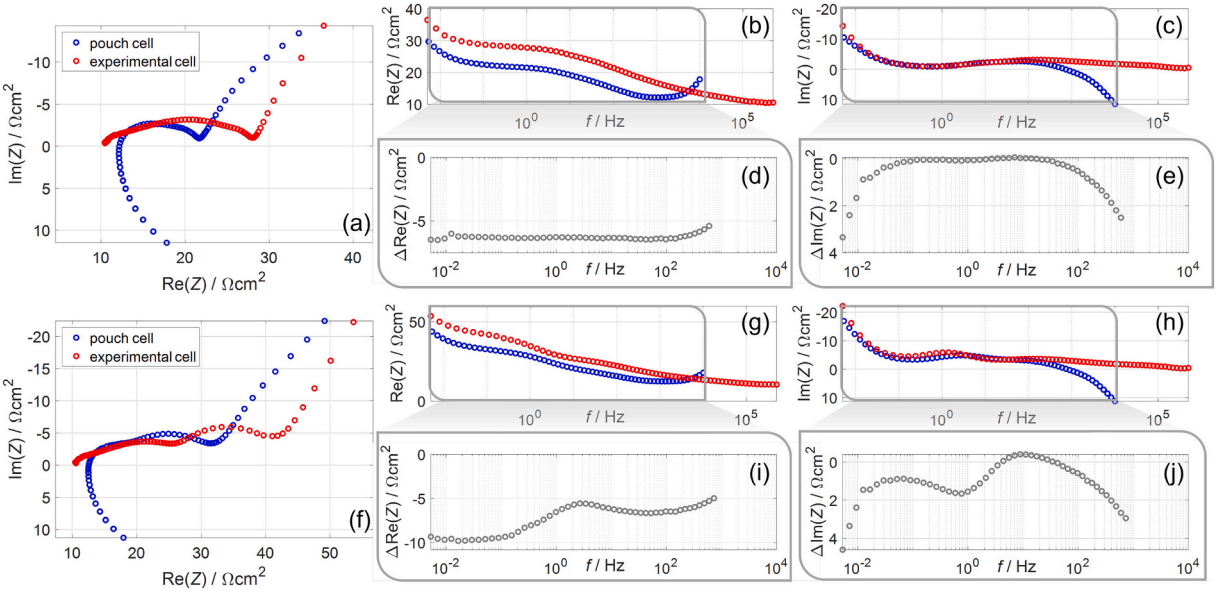

Fig. 6. Comparison of the impedance in the form of Nyquist and Bode plots from pouch and experimental cells, as well as calculated differences in the real and imaginary part for 25 °C and 50 % SoC (a-e) and 25 °C and 10 % SoC (f-j).

As the losses increase with decreasing SoC and the characteristic frequencies of the processes decrease [38,48,49], the differences in the diffusion behavior, due to the different electrolytes, are presumably becoming dominant in the impedance behavior, which leads to the increasing differences of the cells for the lower frequencies.

4.2.2. *Correction factor between experimental and pouch cell*

The comparison between the impedances of both cell types showed that a nearly constant ohmic offset exists for medium SoCs and temperatures, which can be easily corrected by a resistance with the value of the real-part difference. This offset can be explained by the strongly different thicknesses [50] of the separators of the cells and is subsequently physically explicable. This ohmic correction is not quite correct for lower temperatures and SoCs, as the diffusion behavior particularly dominates the losses [26] and, therefore, the difference of the electrolytes leads to a greater deviation. Nevertheless, this constant factor is a first step to an alignment of both cell types for these operation points.

The real part of the averaged impedance of each SoC for the frequencies higher than 2 Hz is calculated and the difference for both cell types is determined for the calculation of this factor. The frequency of 2 Hz is used to ensure that the differences in diffusive behavior are not included in the calculation in order to obtain a purely ohmic correction factor. Utilizing this approach, one ohmic correction value is calculated for each temperature and SoC. This ohmic correction factor can easily be implemented for the simulation model.

4.2.3. *Performance*

Different measurement procedures investigating the voltage behavior were performed for a comparison of the performance of both cell types. Beside different C-rates for charge and discharge, different pulse profiles and driving cycles, such as the WLTP, were also performed. Selected examples at 25 °C of these studies for different C-rates

and one pulse profile are shown in Fig. 7.

Both cell types correlate very well for low C-rates, such as the C/40 in Fig. 7 (a) discharge shown. Only very small deviations for lower SoCs can be seen. This is valid for C-rates below about C/4.

The deviations between the cell types increase strongly for higher C-rates. For the latter, such as the 1C shown in Fig. 7 (b), the overvoltage in the experimental cells is drastically higher than in the pouch cell and the charging is stopped at a SoC which is 10 % lower than in the pouch cell. The existing differences in the separator and electrolyte for higher currents have a distinctly higher influence and, presumably, the clearly higher thickness of the separator in the experimental cell is especially the limiting factor [50]. The electrical contact of the coins is also not optimal with a planar metallic plunger and might cause higher losses [2,51].

An extremely large deviation of the cell types can be observed for dynamic profiles, such as the pulse profile with C/4, C/2, 1C, 1.5C and 2C charge and discharge shown in Fig. 7 (c). This is especially clear for the 'drop' at the beginning of the pulses, which is mainly due to the ohmic resistance. As shown previously in the impedance comparison, the ohmic resistance of the experimental cells is higher, and this results in the higher initial overvoltage of the experimental cells.

The differences between the cells increase, according to the impedance comparisons, with lower SoCs and temperatures. The differences in the separators and electrolytes in the setup for higher currents, together with the contacting, become more noticeable and begin to limit the performance of the experimental cells. This leads to a significant deviation between both cell types in the experimental measurements of the voltage behavior.

4.3. Simulation results

The model introduced for the simulations is used with the experimental current as the input parameter and the simulated voltage as the output. The simulation model of the pouch cell is parameterized as described, based on experimental cell data of the two half-cells' anode and cathode and the correction factor derived is applied. Four different cases for exemplary results are shown in Fig. 8.

For the pulses, the simulation case without correction factor is shown as an example. The strong deviation in the ohmic resistance between both cell types is distinctly visible for the pulses and it is clear, that the correction factor introduced is required to align the experimental cell impedances to the pouch cell. All discussed results are always gained with the complete model inclusive correction factor. A very good agreement between the simulation and measurement can be seen for both cases at 25 °C. The averaged error of the simulated voltage with correction is 0.7 mV (maximal error is 4 mV, which corresponds to 0.1 %) for the pulses (Fig. 8 a) and 1.4 mV (maximal error 9 mV, which corresponds to 0.2 %) for the WLTP (Fig. 8 b).

For lower temperatures the differences between the simulation and measurement increase. For the pulses at 10 °C (Fig. 8 c) the averaged error is 1.1 mV (maximal error 38 mV, which corresponds to 0.96 %). Furthermore, a difference in the relaxation behavior can be seen which results from the different frequency behavior between experimental cells and the pouch cell. For the 1C discharge at 10 °C (Fig. 8 d) the averaged error is 23.9 mV (maximal error 54 mV, which corresponds to 1.6 %). At the constant current simulations, the typical form of the OCV with plateaus and peaks can be seen, which is a weakness of simulations, that do not include inhomogeneities within the cells.

The simulation for 25 °C matches the measurement very well for fast current changes. However, if a constant current is applied for a longer period of time, the simulation underestimates the losses and there is a greater deviation. In these cases, the diffusive processes clearly predominate, which are less well matched by the experimental cell data and the only ohmic correction factor derived in contrast to the other processes. This is an expected result as it correlates with the differences in the impedances mainly due to the different electrolytes and separators of both cell types.

Furthermore, the lowest frequency of the measured impedances is 5 mHz, which is not low enough to assume that the diffusion is completely covered within the impedance. This is particularly the case for the lower SoC and temperatures, which is why diffusion is more difficult to model for these conditions. Nevertheless, for lower temperatures also quite good results can be achieved with the developed fast simulation model, although the errors increase corresponding to the differences in impedance as shown in 4.2.1. Additional simulation cases (constant current charge at 25 °C and one WLTP at 10 °C and one at 0 °C) can be seen in the supplemental figure.

A dynamic current occurs much more frequently than a constant current over a longer period of time for typical applications in an electrical vehicle. Furthermore, charging strategies for fast charging are based on pulses and current reductions when certain criteria are reached [2] and typically take place at temperatures of at least 25 °C. Current changes and pulses are already well represented by the model. The remaining inaccuracy of the model for the scenarios described is, thus, not limiting and the model already enables reliable and faster than real-time predictions for a broad spectrum of operating scenarios.

5. Conclusion

The measurement of significant half-cell impedance spectra for the individual electrodes extracted from an automotive pouch cell with an experimental test cell setup from EL-Cell is shown in this work, along with the methodologies needed to build the test cells and determine significant data. We proved that the combination of the half-cell impedances resembles the full cell behavior correctly, underlining the capability of the methodology presented.

Thereby, the inductive loop, as observed in the literature, in the impedance of the anode and cathode of experimental cell setups was further investigated. We showed by comprehensive measurements that this is probably caused by the specifics of the Li reference ring of the experimental setup as well as the different magnitudes of the impedances of the electrodes and not by physical processes at the electrodes.

The measurements of the experimental cell setup with a standard separator and electrolyte and the automotive pouch cells show a very good accordance between both cell types for medium SoCs and temperatures for the impedance behavior and for medium C-rates for the

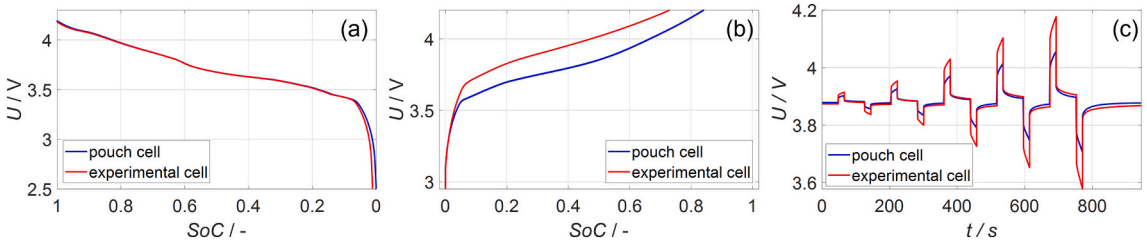

Fig. 7. Comparison of the voltage behavior of both cell types for different cases at 25 °C: quasi-OCV C/40 discharge (a), 1C charge (b) and a pulse profile for pulses with C/4, C/2, 1C, 1.5C and 2C at 70 % SoC (c).

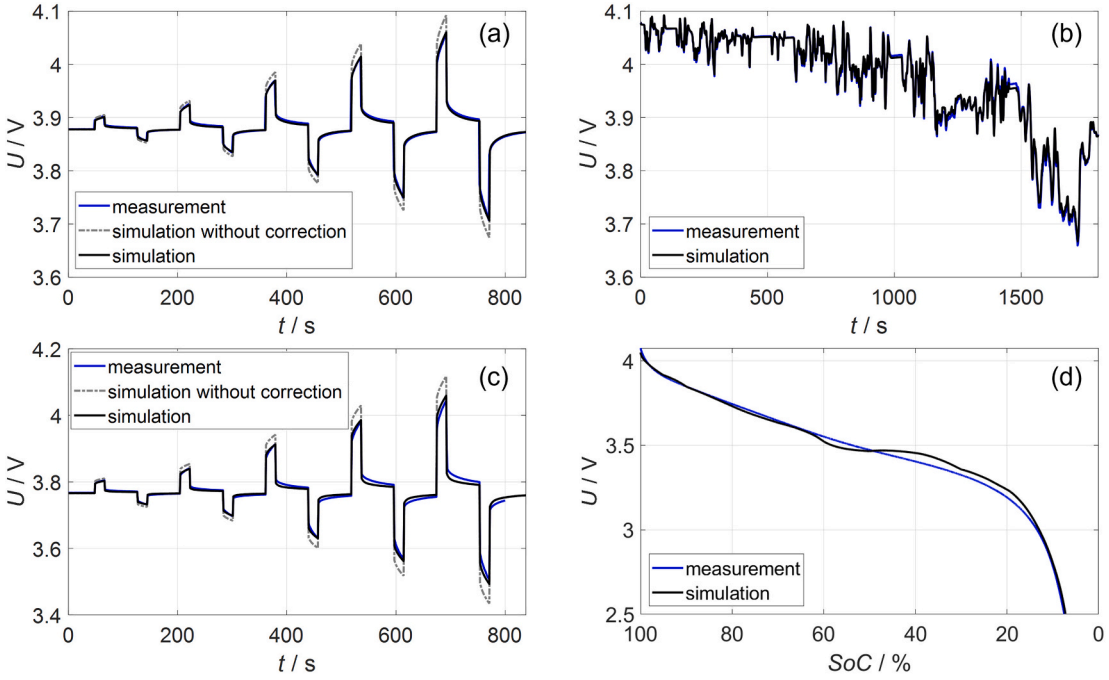

Fig. 8. Comparison of a pouch cell measurement and a simulation of the model for two cases at 25 °C. (a) 18 s Pulses with currents C/4, C/2, 1C, 1.5C and 2C at 70 % SoC and (b) a WLTP cycle at 90 % SoC. And for two cases at 10 °C. (c) 18 s Pulses with currents C/4, C/2, 1C, 1.5C and 2C at 60 % SoC and (d) a constant current discharge with 1C.

performance. The impedances still differ from each other, especially for lower SoCs and temperatures, where presumably the existing differences in the setup of the cells in the electrolyte and separator dominate.

The fitted impedances of the anode and cathode from experimental cell measurements, together with the ohmic correction factor derived and the OCVs, form the basis for a simple and efficient simulation model in MATLAB for the replication of the voltage behavior of the automotive pouch cell. The simulated pouch cell behavior for fast changing current loads, such as pulse profiles or WLTP, correlates very well with the measurements, whereas the deviation increases for constant currents over a longer period of time.

This work showed that a very good simulation of the pouch cell behavior can be performed with parameterization from experimental cell measurements using a standardized separator and electrolyte. By building the model based on the individual electrode data gained from a full cell configuration with reference electrode, statements can be made about the limiting electrode in certain application scenarios, such as fast charging. This represents a significant improvement over a simulation model that is parameterized only on the pouch cell level, neglecting the individual process on the anode and cathode.

The replication quality achieved using the correction factor derived is particularly noteworthy as only the electrodes are extracted from the pouch cell and standard components for the separator and electrolyte are used in the commercial experimental cell setup, seemingly a strong deviation from the pouch cell. This shows a good potential for fast and meaningful parametrization of simulation models without the need for a detailed replication of these very difficult to identify and access cell components. At the same time, the experimental cell setup benefits from the Li reference electrode enabling measurement of half-cell data without much effort, which can hardly be implemented in automotive pouch cells without changing their behavior.

A better correspondence between the pouch cell and the experimental cell impedances outside of the medium temperatures and SoCs is also required for a higher accuracy of the model. At the same time, this would probably also increase the compliance for constant current loads. A systematic variation of the experimental cell setup will be investigated in a future study for this purpose.

Batteries in applications like electrical vehicles are rarely exposed to homogeneous boundary conditions like temperatures. The inhomogeneous temperatures in turn lead to inhomogeneous electrochemical behavior in the cell. To take inhomogeneous temperatures and SoCs at different parts of the large-format pouch cell into account, the model will be spatially resolved in a next step and additionally coupled with a thermal model.

Furthermore, this methodology should be applied to other cell chemistries and cell formats in order to make a more general statement about whether this approach can be universally applied. Additionally, for long-term performance analysis of the battery, it is essential to incorporate degradation mechanisms, such as the increase in the solid electrolyte interphase (SEI) or dendrite growth, into the model, thereby enabling long-term predictions of battery behavior.

Supplementary data to this article can be found online at https://doi.org/10.1016/j.est.2025.116812.

CRediT authorship contribution statement

Anne Heß: Writing – original draft, Visualization, Validation, Software, Project administration, Methodology, Investigation, Formal analysis, Data curation, Conceptualization. **Thomas Wetzel:** Writing – review & editing, Supervision, Resources, Project administration, Funding acquisition. **Philipp Seegert:** Writing – review & editing, Supervision, Resources, Project administration, Funding acquisition, Conceptualization.

Declaration of competing interest

The authors declare that they have no known competing financial interests or personal relationships that could have appeared to influence the work reported in this paper.

Acknowledgements

We thank Sabrina Herberger (KIT, TVT) for her support of this work. We gratefully thank and acknowledge the Schaeffler Technologies AG &

Co. KG for funding and thank especially Daniel Werner and Jürgen Remmlinger from SHARE at KIT for their valuable input and the helpful discussions.

Data availability

Data will be made available on request.

References

[1] T. Waldmann, B.-I. Hogg, M. Wohlfahrt-Mehrens, Li plating as unwanted side reaction in commercial Li-ion cells – a review, J. Power Sources 384 (2018) 107–124, https://doi.org/10.1016/j.jpowsour.2018.02.063.

[2] N. Wassiliadis, M. Ank, L. Wildfeuer, M.K. Kick, M. Lienkamp, Experimental investigation of the influence of electrical contact resistance on lithium-ion battery testing for fast-charge applications, Appl. Energy 295 (2021) 117064, https://doi.org/10.1016/j.apenergy.2021.117064.

[3] F.F. Oehler, X. Deuschl, K. Nürnberger, A. Graule, S. Kücher, T. Roth, A. Adam, J. Li, R. Mörtel, A. Jossen, Online adaptive anode potential-controlled fast charging of lithium-ion cells using a validated electrochemical model-based virtual reference electrode, J. Power Sources 608 (2024) 234620, https://doi.org/10.1016/j.jpowsour.2024.234620.

[4] A. Kayyar, J. Huang, M. Samiee, J. Luo, Construction and testing of coin cells of lithium ion batteries, JoVE (2012) 4104, https://doi.org/10.3791/4104.

[5] S.E. Trask, Y. Li, J.J. Kubal, M. Bettge, B.J. Polzin, Y. Zhu, A.N. Jansen, D. P. Abraham, From coin cells to 400 mAh pouch cells: enhancing performance of high-capacity lithium-ion cells via modifications in electrode constitution and fabrication, J. Power Sources 259 (2014) 233–244, https://doi.org/10.1016/j.jpowsour.2014.02.077.

[6] B.R. Long, S.G. Rinaldo, K.G. Gallagher, D.W. Dees, S.E. Trask, B.J. Polzin, A. N. Jansen, D.P. Abraham, I. Bloom, J. Bareño, J.R. Croy, Enabling high-energy, high-voltage lithium-ion cells: standardization of coin-cell assembly, electrochemical testing, and evaluation of full cells, J. Electrochem. Soc. 163 (2016) A2999–A3009, https://doi.org/10.1149/2.0691614jes.

[7] S. Chen, C. Niu, H. Lee, Q. Li, L. Yu, W. Xu, J.-G. Zhang, E.J. Dufek, M. S. Whittingham, S. Meng, J. Xiao, J. Liu, Critical parameters for evaluating coin cells and pouch cells of rechargeable Li-metal batteries, Joule 3 (2019) 1094–1105, https://doi.org/10.1016/j.joule.2019.02.004.

[8] V. Murray, D.S. Hall, J.R. Dahn, A guide to full coin cell making for academic researchers, J. Electrochem. Soc. 166 (2019) A329–A333, https://doi.org/10.1149/2.1171902jes.

[9] D. Schreiner, T. Zünd, F.J. Günter, L. Kraft, B. Stumper, F. Linsenmann, M. Schüßler, R. Wilhelm, A. Jossen, G. Reinhart, H.A. Gasteiger, Comparative evaluation of LMR-NCM and NCA cathode active materials in multilayer lithium-ion pouch cells: part I. Production, electrode characterization, and formation, J. Electrochem. Soc. 168 (2021) 030507, https://doi.org/10.1149/1945-7111/abe50c.

[10] L. Kraft, T. Zünd, D. Schreiner, R. Wilhelm, F.J. Günter, G. Reinhart, H. A. Gasteiger, A. Jossen, Comparative evaluation of LMR-NCM and NCA cathode active materials in multilayer lithium-ion pouch cells: part II. Rate capability, long-term stability, and thermal behavior, J. Electrochem. Soc. 168 (2021) 020537, https://doi.org/10.1149/1945-7111/abe5e6.

[11] G. Bridgewater, M.J. Capener, J. Brandon, M.J. Lain, M. Copley, E. Kendrick, A comparison of lithium-ion cell performance across three different cell formats, Batteries 7 (2021) 38, https://doi.org/10.3390/batteries7020038.

[12] M.D.L. Garayt, M.B. Johnson, L. Laidlaw, M.A. McArthur, S. Trussler, J.E. Harlow, J.R. Dahn, C. Yang, A guide to making highly reproducible Li-ion single-layer pouch cells for academic researchers, J. Electrochem. Soc. 170 (2023) 080516, https://doi.org/10.1149/1945-7111/aceffc.

[13] A. Smith, P. Stüble, L. Leuthner, A. Hofmann, F. Jeschull, L. Mereacre, Potential and limitations of research battery cell types for electrochemical data acquisition, Batteries Supercaps 6 (2023) e202300080, https://doi.org/10.1002/batt.202300080.

[14] Y. Son, H. Cha, T. Lee, Y. Kim, A. Boies, J. Cho, M. De Volder, Analysis of differences in electrochemical performance between coin and pouch cells for lithium-ion battery applications, Energy Environ. Mater. 7 (2024) e12615, https://doi.org/10.1002/eem2.12615.

[15] S. Schindler, M.A. Danzer, Influence of cell design on impedance characteristics of cylindrical lithium-ion cells: a model-based assessment from electrode to cell level, J. Energy Storage 12 (2017) 157–166, https://doi.org/10.1016/j.est.2017.05.002.

[16] J. Illig, M. Ender, A. Weber, E. Ivers-Tiffée, Modeling graphite anodes with serial and transmission line models, J. Power Sources 282 (2015) 335–347, https://doi.org/10.1016/j.jpowsour.2015.02.038.

[17] J. Costard, J. Joos, A. Schmidt, E. Ivers-Tiffée, Charge Transfer Parameters of $Ni_x Mn_y Co_{1-x-y}$ Cathodes Evaluated by a Transmission Line Modeling Approach, Energy Tech. 9 (2021) 2000866, https://doi.org/10.1002/ente.202000866.

[18] A.U. Schmid, A. Ridder, M. Hahn, K. Schofer, K.P. Birke, Aging of extracted and reassembled Li-ion electrode material in coin cells—capabilities and limitations, Batteries 6 (2020) 33, https://doi.org/10.3390/batteries6020033.

[19] J. Song, Two- and three-electrode impedance spectroscopy of lithium-ion batteries, J. Power Sources 111 (2002) 255–267, https://doi.org/10.1016/S0378-7753(02)00310-5.

[20] M. Itagaki, N. Kobari, S. Yotsuda, K. Watanabe, S. Kinoshita, M. Ue, In situ electrochemical impedance spectroscopy to investigate negative electrode of lithium-ion rechargeable batteries, J. Power Sources 135 (2004) 255–261, https://doi.org/10.1016/j.jpowsour.2004.04.004.

[21] C. Huang, S. Zhuang, F. Tu, Electrode/electrolyte interfacial behaviors of $LiCoO_2$ /mixed graphite Li-ion cells during operation and storage, J. Electrochem. Soc. 160 (2013) A376–A382, https://doi.org/10.1149/2.009303jes.

[22] Y. Hoshi, Y. Narita, K. Honda, T. Ohtaki, I. Shitanda, M. Itagaki, Optimization of reference electrode position in a three-electrode cell for impedance measurements in lithium-ion rechargeable battery by finite element method, J. Power Sources 288 (2015) 168–175, https://doi.org/10.1016/j.jpowsour.2015.04.065.

[23] S.J. An, J. Li, C. Daniel, S. Kalnaus, D.L. Wood, Design and demonstration of three-electrode pouch cells for lithium-ion batteries, J. Electrochem. Soc. 164 (2017) A1755–A1764, https://doi.org/10.1149/2.0031709jes.

[24] J.S. Gnanaraj, R.W. Thompson, S.N. Iaconatti, J.F. DiCarlo, K.M. Abraham, Formation and growth of surface films on graphitic anode materials for Li-ion batteries, Electrochem. Solid St. 8 (2005) A128, https://doi.org/10.1149/1.1850390.

[25] B. Zhang, L. Wang, Y. Zhang, X. Wang, Y. Qiao, S.-G. Sun, Reliable impedance analysis of Li-ion battery half-cell by standardization on electrochemical impedance spectroscopy (EIS), J. Chem. Phys. 158 (2023) 054202, https://doi.org/10.1063/5.0139347.

[26] S. Gantenbein, M. Weiss, E. Ivers-Tiffée, Impedance based time-domain modeling of lithium-ion batteries: part I, J. Power Sources 379 (2018) 317–327, https://doi.org/10.1016/j.jpowsour.2018.01.043.

[27] EL-Cell GmbH. https://el-cell.com/products/test-cells/standard-test-cells/pat-cell/, 2024. (Accessed 1 October 2024).

[28] S. Buller, M. Thele, R.W.A.A. DeDoncker, E. Karden, Impedance-based simulation models of supercapacitors and Li-ion batteries for power electronic applications, IEEE Trans. Ind. Applicat. 41 (2005) 742–747, https://doi.org/10.1109/TIA.2005.847280.

[29] D. Andre, M. Meiler, K. Steiner, H. Walz, T. Soczka-Guth, D.U. Sauer, Characterization of high-power lithium-ion batteries by electrochemical impedance spectroscopy. II: modelling, J. Power Sources 196 (2011) 5349–5356, https://doi.org/10.1016/j.jpowsour.2010.07.071.

[30] M. Schönleber, E. Ivers-Tiffée, Approximability of impedance spectra by RC elements and implications for impedance analysis, Electrochem. Commun. 58 (2015) 15–19, https://doi.org/10.1016/j.elecom.2015.05.018.

[31] H. Nara, D. Mukoyama, T. Yokoshima, T. Momma, T. Osaka, Impedance analysis with transmission line model for reaction distribution in a pouch type lithium-ion battery by using micro reference electrode, J. Electrochem. Soc. 163 (2016) A434–A441, https://doi.org/10.1149/2.0341603jes.

[32] J. Bisquert, G. Garcia-Belmonte, F. Fabregat-Santiago, A. Compte, Anomalous transport effects in the impedance of porous film electrodes, Electrochem. Commun. 1 (1999) 429–435, https://doi.org/10.1016/S1388-2481(99)00084-3.

[33] J. Euler, W. Nonnenmacher, Stromverteilung in porösen elektroden, Electrochim. Acta 2 (1960) 268–286, https://doi.org/10.1016/0013-4686(60)80025-4.

[34] R. De Levie, On porous electrodes in electrolyte solutions—IV, Electrochim. Acta 9 (1964) 1231–1245, https://doi.org/10.1016/0013-4686(64)85015-5.

[35] J. Costard, Einfluss von Mikrostruktur und Materialparametern auf die Leistungsfähigkeit poröser Elektroden für Lithium-Ionen Batterien, 2018.

[36] M. Ender, A. Weber, E. Ivers-Tiffée, A novel method for measuring the effective conductivity and the contact resistance of porous electrodes for lithium-ion batteries, Electrochem. Commun. 34 (2013) 130–133, https://doi.org/10.1016/j.elecom.2013.05.037.

[37] J. Schmalstieg, Physikalisch-elektrochemische Simulation von Lithium-Ionen-Batterien Implementierung, Parametrierung und Anwendung, 2017.

[38] J. Illig, Physically Based Impedance Modelling of Lithium-Ion Cells, 2014.

[39] B. Hauck, Impedanzbasierte Spannungsprädiktion von Lithium-Ionen-Batterien, 2024.

[40] M. Ecker, T.K.D. Tran, P. Dechent, S. Käbitz, A. Warnecke, D.U. Sauer, Parameterization of a physico-chemical model of a lithium-ion battery: I. Determination of parameters, J. Electrochem. Soc. 162 (2015) A1836–A1848, https://doi.org/10.1149/2.0551509jes.

[41] M. Weiss, Impedanzgestützte Lebensdaueranalyse von Lithium-Ionen Batterien, 2020.

[42] M. Ender, Mikrostrukturelle Charakterisierung, Modellentwicklung und Simulation poröser Elektroden für Lithiumionenzellen, 2014.

[43] M. Wünsch, R. Füßler, D.U. Sauer, Metrological examination of an impedance model for a porous electrode in cyclic aging using a 3-electrode lithium-ion cell with NMC111 | graphite, J. Energy Storage 20 (2018) 196–203, https://doi.org/10.1016/j.est.2018.09.010.

[44] B.A. Boukamp, Interpretation of an 'Inductive Loop' in the Impedance of an Oxygen Ion Conducting Electrolyte/metal Electrode System, Solid State Ionics 143 (2001) 47–55, https://doi.org/10.1016/S0167-2738(01)00832-3.

[45] F. Dinkelacker, P. Marzak, J. Yun, Y. Liang, A.S. Bandarenka, Multistage mechanism of lithium intercalation into graphite anodes in the presence of the solid electrolyte interface, ACS Appl. Mater. Interfaces 10 (2018) 14063–14069, https://doi.org/10.1021/acsami.7b18738.

[46] A. Thapa, H. Gao, Low-frequency inductive loop and its origin in the impedance spectrum of a graphite anode, J. Electrochem. Soc. 169 (2022) 110535, https://doi.org/10.1149/1945-7111/aca364.

[47] H. Brandstätter, I. Hanzu, M. Wilkening, Myth and reality about the origin of inductive loops in impedance spectra of lithium-ion electrodes — a critical experimental approach, Electrochim. Acta 207 (2016) 218–223, https://doi.org/10.1016/j.electacta.2016.03.126.

[48] J.P. Schmidt, P. Berg, M. Schönleber, A. Weber, E. Ivers-Tiffée, The distribution of relaxation times as basis for generalized time-domain models for Li-ion batteries, J. Power Sources 221 (2013) 70–77, https://doi.org/10.1016/j.jpowsour.2012.07.100.
[49] P. Iurilli, C. Brivio, R. Carrillo, V. Wood, EIS2MOD: a DRT-based modeling framework for Li-ion cells, IEEE Trans. on Ind. Applicat. 58 (2022) 1429–1439, https://doi.org/10.1109/TIA.2021.3134946.
[50] D.V. Horváth, R. Tian, C. Gabbett, V. Nicolosi, J.N. Coleman, Quantifying the effect of separator thickness on rate performance in lithium-ion batteries, J. Electrochem. Soc. 169 (2022) 030503, https://doi.org/10.1149/1945-7111/ac5654.
[51] P. Taheri, S. Hsieh, M. Bahrami, Investigating electrical contact resistance losses in lithium-ion battery assemblies for hybrid and electric vehicles, J. Power Sources 196 (2011) 6525–6533, https://doi.org/10.1016/j.jpowsour.2011.03.056.